



Cite this: DOI: 10.1039/c4gc01052c

Efficient biomass transformations catalyzed by graphene-like nanoporous carbons functionalized with strong acid ionic liquids and sulfonic groups†

Fujian Liu,^{a,b} Weiping Kong,^a Liang Wang,^b Xianfeng Yi,^c Iman Noshadi,^d Anmin Zheng^{*c} and Chenze Qi^{*a}

Strong acid ionic liquids and sulfonic group bifunctional graphene-like nanoporous carbons (GNC-SO₃H-ILs) have been synthesized by treating nitrogen containing graphene-like nanoporous carbons (GNCs) with 1,3-propanesultone, ion exchanging with HSO₃CF₃ or H₂SO₄. Introducing nitrogen is important for grafting strong acid ionic liquids and sulfonic group in GNCs, which were synthesized from carbonization of a mixture of dicyandiamide or melamine and glucose. GNC-SO₃H-ILs possess abundant nanopores, nanosheet structure, good dispersion and controlled acidity. By themselves, they are capable of enhancing the fast diffusion of reactants and products, while increasing the exposure degree of acidic sites in GNC-SO₃H-ILs throughout various reactions. The above characteristics resulted in their much improved catalytic activity in biomass transformations such as the production of biodiesel and depolymerization of crystalline cellulose into sugars, which was even comparable to those of homogeneous ionic liquid and mineral acids.

Received 7th June 2014,
Accepted 11th September 2014

DOI: 10.1039/c4gc01052c

www.rsc.org/greenchem

1. Introduction

Great effort has been made to develop efficient and cost effective ways to transform biomass into biofuels, due to the low cost, excellent renewability and environmental friendliness of biomass when compared with conventional fossil energy.^{1–9} Biomass may therefore be the most important feedstock for replacing conventional fossil energy in the future. Generally, biofuels were typically produced by two routes: (i) towards transesterification to biodiesel and (ii) depolymerization of crystalline cellulose into sugars and fine chemicals.^{1,2,7,10–15} Notably, biodiesel production was focused on employing low cost and low quality plant oil or waste oil as the feedstocks, typically held under green and mild conditions.¹⁶ Alternatively, the depolymerization of cellulose was mostly held under

severe conditions.^{7,9} Surprisingly, crystalline cellulose easily transformed into sugars in the presence of alkylmethylimidazolium ionic liquid solvents because of their unique ability to break down the crystalline cellulose into soluble polymer chains. However, the high cost of ionic liquids and the reaction mixtures' acute recyclability create a demand for new catalysts with extremely high effectiveness. Researchers have discovered that acids, bases or enzyme catalysts were active when producing biomass transformations.^{1,2,7,10–16} Acid catalysts were highly efficient and low in cost for biomass transformation, which could catalyze the transformation of low-quality and low cost biomass into biofuels under rather mild conditions. The replacement of mineral acids with solid acids in terms of biomass transformation has received considerable attention regarding green and sustainable chemistry.^{10–19}

Among various heterogeneous acid catalysts, carbon based solid acids showed controlled wettability, good thermal and chemical stabilities and superior catalytic activity throughout various reactions, combining the advantages of the solid acids with both organic and inorganic frameworks.^{3,20–24} Graphene based nanomaterials act as novel carbon materials. Materials scientists, chemists and physicist recognize that these materials possess excellent thermal and mechanical stabilities, unique nanosheet structure, controlled wettability and very good dispersion in various systems.^{25–30} These are the ideal candidates for solid acidic catalysts or catalyst supports because they are capable of largely reducing the limitation of

^aKey Laboratory of Alternative Technologies for Fine Chemicals Process of Zhejiang Province, Department of Chemistry, Shaoxing University, Shaoxing, 312000, China. E-mail: qichenze@usx.edu.cn

^bDepartment of Chemistry, Zhejiang University (XiXi Campus), Hangzhou, 310028, China

^cWuhan Center for Magnetic Resonance, State Key Laboratory of Magnetic Resonance and Atomic and Molecular Physics, Wuhan Institute of Physics and Mathematics, Chinese Academy of Sciences, Wuhan 430071, China.

E-mail: zhenganm@wipm.ac.cn

^dPolymer Program, Institute of Materials Science and Department of Chemistry, University of Connecticut, Storrs, CT 06269, USA

† Electronic supplementary information (ESI) available. See DOI: 10.1039/c4gc01052c

mass transfer, increase the exposure degree of active sites and enhance the recyclability of the catalysts in various reactions.^{31–33} Due to the frequency of graphene nanomaterial layers sticking together, it is imperative to create pillars between the layers, maximizing the surface area and accessibility during various reactions.^{31–33} Still, the synthesis of graphene based nanomaterials with large BET surface areas and abundant nanopores through facile and cost-effective routes remains a challenge.^{34–38} Abundant nanopores in graphene-based nanomaterials must be created to increase the degree of active sites, which contribute importantly to their application during heterogeneous catalysis.³¹

We report here the successful synthesis of novel acid ionic liquids and sulfonic group bifunctional graphene-like nanoporous carbons (GNC-SO₃H-ILs), which were synthesized by treating nitrogen containing graphene-like nanoporous carbons (GNCs) with 1,3-propanesultone. The anions were exchanged with strong acids of H₂SO₄ or HSO₃CF₃. The introduction of nitrogen atoms into GNCs forms strong acid ionic liquids and sulfonic groups through the quaternary ammonization reaction. The GNC supports could be easily synthesized using a one-step carbonization mixture. This mixture should consist of dicyandiamide/melamine and glucose, using no additional templates (as shown in Scheme 1). The resulting bifunctional carbon based solid acids showed controlled acidity, unique nanosheet structure, abundant nanopores and good stability. Interestingly, GNC-SO₃H-ILs showed significantly improved catalytic activity and good recyclability in biomass transformation, including transesterification to biodiesel and depolymerization of crystalline cellulose into sugars and 5-hydroxymethylfurfural (HMF). This process was better than those of acidic resin of Amberlyst 15, sulfonic group functionalized mesoporous SBA-15, and heteropolyacid of H₃PW₁₂O₄₀, which was even comparable to those of homogeneous acid ionic liquids and mineral acids. The preparation of GNC-SO₃H-ILs fosters a facile and cost-effective method to synthesize highly efficient graphene based solid acids for biomass transformation, which is crucial for their various

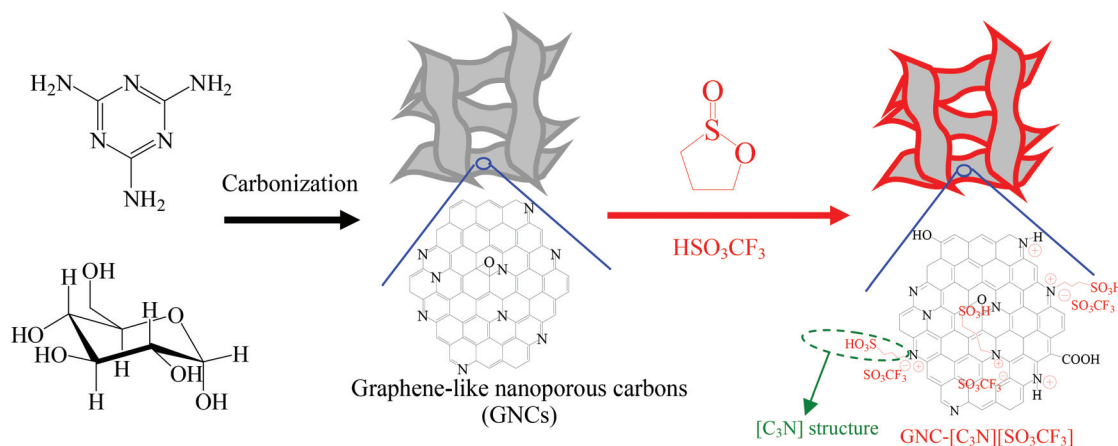
applications when exploring biofuel through green and sustainable processes.

2. Experimental details

2.1 Preparation of catalysts

2.1.1 Synthesis of GNCs. GNCs were synthesized from carbonization of the mixture of melamine and glucose with various weight ratios under N₂ conditions. Typically, 0.1 g of glucose and 4.0 g of melamine were mixed together. After grinding the mixture for 10 minutes, the sample was transferred into the tube furnace under flowing N₂ conditions. The temperature of the tube furnace experienced the following heating processes: from room temperature to 600 °C (2.5 °C min⁻¹), from 600 °C to 800 °C (1.67 °C min⁻¹), and remained at 800 °C for 1 h. After cooling the furnace to room temperature, GNCs with monolithic morphology were obtained. Moreover, GNCs could also be synthesized from carbonization of the mixture of dicyandiamide and glucose using similar weight ratios under similar conditions.

2.1.2 Synthesis of strong acid ionic liquids and sulfonic group bifunctional GNCs (GNC-SO₃H-ILs). GNC-SO₃H-ILs were synthesized from quaternary ammonization of GNCs with 1,3-propanesultone, and anion exchange with strong acids of H₂SO₄ or HSO₃CF₃. As a typical run for the synthesis of GNC-[C₃N][SO₃CF₃], 1.2 g of GNC were added into a mixture containing 20 mL of toluene and 0.3 g of 1,3-propanesultone. After heating the reaction mixture at 110 °C for 24 h under refluxing, the reaction mixture was cooled down to room temperature (25 °C). The sample was then treated with a solution containing 25 mL of toluene and 3–5 mL HSO₃CF₃ for 24 h at room temperature under vigorous stirring. GNC-[C₃N][SO₃CF₃] could be obtained by filtering, washing with a large amount of CH₂Cl₂ to remove the residual HSO₃CF₃, and then drying it at 60 °C for 12 h. This procedure was repeated twice. GNC-[C₃N]-[SO₃CF₃] was then obtained, where [SO₃CF₃] stands for the treating acid of trifluoromethanesulfonic acid and C₃ stands



Scheme 1 The procedures for synthesizing GNC-[C₃N][SO₃CF₃].

for 1,3-propanesultone. The detailed synthetic procedures of GNC-[C₃N][SO₃CF₃] are also shown in Scheme 1. For comparison, [C₃vim][SO₃CF₃] (“C₃” stands for 1,3-propanesultone, “vim” stands for vinyl imidazole and “[SO₃CF₃]” stands for the treating acid of HSO₃CF₃) and SBA-15-SO₃H (S/Si = 0.2, “SBA” stands for ordered mesoporous silica) were synthesized according to the literature.^{8,39}

2.2 Catalytic reactions

2.2.1 Transesterification. Transesterification of tripalmitin with methanol was executed as follows: 0.84 g (1.04 mmol) of tripalmitin was melted into a flask equipped with a condenser and a magnetic stirrer at 65 °C. Then, 0.10 g of catalyst was quickly added under vigorous stirring to form a homogeneous mixture. 2.47 mL (61 mmol) of methanol was then added; after further stirring the mixture for 14 h at 65 °C under refluxing, the reaction was complete; the catalysts could be separated by centrifugation. The molar ratio of tripalmitin/methanol was 1/60 and the mass ratio of catalyst/tripalmitin was 0.119. The product was methyl palmitate with selectivity near 100%, which was analyzed by gas chromatography of Agilent 7890 with a flame ionization detector (FID). The column was a HP-INNOWax capillary column (30 m); the initial temperature was 100 °C, the ramping rate was 20 °C min⁻¹, and the final temperature was 280 °C; the temperature of the FID detector was 350 °C. In this reaction, the concentration of methyl palmitate was calculated through the internal standard (dodecane) method, establishing the standard curve.

Transesterification of sunflower oil with methanol was executed as follows: 1.0 g of sunflower oil (1.16 mmol) was added into a flask equipped with a condenser and a magnetic stirrer. The temperature was rapidly increased to 65 °C. Then, 3.5 mL of methanol (86.3 mmol) and 0.15 g of catalyst were quickly added under vigorous stirring. The reaction occurred for 18 h. The molar ratio of sunflower oil to methanol was 1/75 and the mass ratio of catalyst to tripalmitin was 0.1. The products were mainly methyl palmitate (C_{16:0}), methyl stearate (C_{18:0}), methyl oleate (C_{18:1}), methyl linoleate (C_{18:2}), and methyl heptacosane (C_{27:0}). The quantification of these products was analyzed by using an Agilent GC/MS instrument (Agilent 6890N/5975I) with a programmable split/splitless injector.

2.2.2 Catalysts regeneration. 1.0 g (1.16 mmol) of sunflower oil was melted into a flask equipped with a condenser and a magnetic stirrer at 65 °C. Then, 0.15 g of catalyst was quickly added under vigorous stirring to form a homogeneous mixture; then 3.5 mL (86.3 mmol) of methanol was added; after stirring the mixture for 18 h at 65 °C under reflux, the reaction was complete. Centrifugation was then carried out for catalyst separation. The catalyst was used for the next run after washing the sample with a large amount of CH₂Cl₂, which removed the absorbed reactants and products, and drying the sample under vacuum conditions.

2.2.3 Depolymerization of crystalline cellulose into sugars and HMF. The depolymerization of crystalline cellulose from Avicel was also chosen as the model reaction for evaluating the activities of various catalysts. As a typical run for depolymerization

of Avicel, 100 mg of crystalline cellulose of Avicel was dissolved in a mixture containing 1.5 g of [C₄mim]Cl ionic liquid and 0.5 mL of DMSO at 100 °C for 3–5 h under vigorous stirring until a clear solution was obtained, followed by an additional 20 mg of GNC-[C₃N][SO₃CF₃]. Then, 600 μL of water was slowly introduced into the reaction mixture while the reaction temperature remained at 100 °C. At different time intervals, samples were withdrawn, weighed, quenched immediately with cold water, and centrifuged at 14 800 rpm for 5 min to remove catalysts and unreacted cellulose, giving the reaction mixture. Various acid catalysts such as Amberlyst 15, HCl and [C₃vim][SO₃CF₃] were also used for catalyzing depolymerization of Avicel, which used the same number of acidic sites as in GNC-[C₃N][SO₃CF₃].

Meanwhile, the isolated cellulose was thoroughly washed with water, and recovered through centrifugation. The amount of cellulose isolated was determined by weight.

2.2.4 Testing total reducing sugar (TRS). TRS value was usually used for evaluating the depolymerization degree of crystalline cellulose catalyzed by various catalysts, which was tested through the DNS method.^{7,9,14} As a typical run, a mixture containing 0.5 mL of 3,5-dinitrosalicylic acid (DNS) reagent and 0.5 mL of reaction mixture was heated for 5 min at 100 °C and then cooled to room temperature. Then, 4 mL of deionized water was added to dilute the mixture. The color intensity of the mixture was measured on a NanoDrop 2000 UV-spectrophotometer at 540 nm. The concentration of the total reducing sugars was calculated based on a standard curve obtained with glucose.

The concentrations of glucose and cellobiose in the reaction mixture were measured using the Shimadzu LC-20A HPLC system based on the standard curve method, which was equipped with a SCR-101N column using extra-pure water during the mobile phase at a flow rate of 0.5 mL min⁻¹. The column's temperature was set to 55 °C. In the meantime, a refraction index was used for the detection of sugars in the water. The concentration of 5-hydroxymethylfurfural (HMF) was also measured using a Shimadzu LC-20A HPLC system based on the standard curve method. It was equipped with a CAPCELL PAK C18 column using methanol and water (methanol–water = 80 : 20) during the mobile phase, at a flow rate of 0.7 mL min⁻¹, and the column's temperature was set to 50 °C. At the same time, an ultraviolet detector with the wavelength number at 254 nm was used for the detection of HMF in the reaction mixture.

3. Results and discussion

3.1 Structural characterization

Fig. 1A shows XRD patterns of GNC and GNC-[C₃N][SO₃CF₃]. Notably, GNC exhibits two broad peaks centered at 26.1 and 43.2°. These are associated with the graphite structure, which was extremely close to the peaks of graphene based nanomaterials with a nanosheet structure, reported previously.^{31,37} This result indicated that graphene-like structures with several

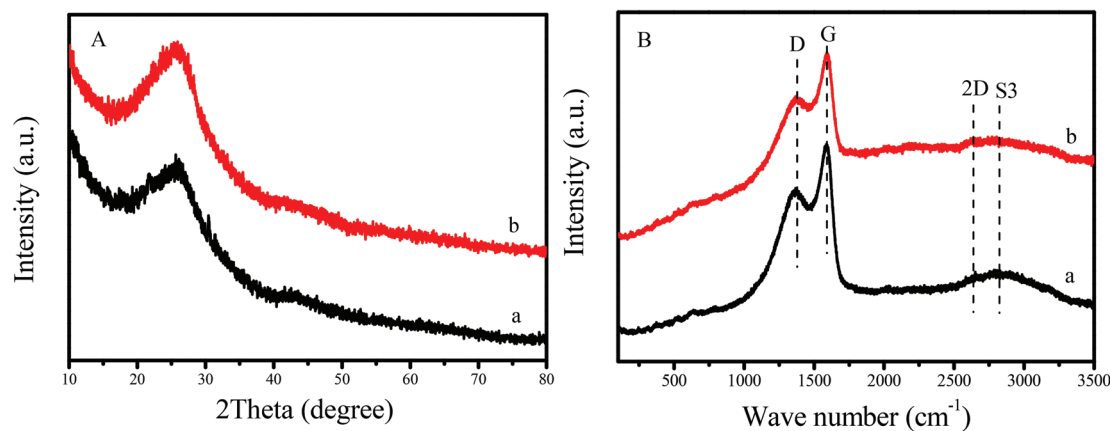


Fig. 1 (A) XRD patterns and (B) Raman spectra of (a) GNC and (b) GNC-[C₃N][SO₃CF₃].

layers was formed in the GNC. After grafting the strong acid ionic liquids and the sulfonic group onto the network of GNC, the sample of GNC-[C₃N][SO₃CF₃] was given, which showed almost no change in XRD patterns compared to the GNC support. The above results indicated that the graphene-like nanosheet structure was well maintained in GNC-[C₃N][SO₃CF₃].

In addition, the graphene-like structures of GNC and GNC-[C₃N][SO₃CF₃] have also been confirmed by Raman spectra. It is well known that Raman spectroscopy is a powerful approach for determining the properties of graphene based nanomaterials such as the number and orientation of layers, the quality and types of edges and the effects of perturbations involving the structure strain, doping, disorder and functional groups.^{40,41} Fig. 1B shows the Raman spectra of GNC and GNC-[C₃N][SO₃CF₃]. It was noted that a series of peaks at approximately 1378, 1591, 2639 and 2822 cm⁻¹ were clearly observed in these samples, which could be attributed to the signals of D, G, 2D and S3 bands.²⁶ The broadened D-band indicated the presence of sp³ carbon atoms with defects and disorders at the edges and the boundaries of the graphene domains. The sharp G-band indicated the presence of sp² carbon atoms in a graphitic 2D hexagonal lattice, confirming the formation of graphitic carbon, in good agreement with

XRD results. Compared with GNC, GNC-[C₃N][SO₃CF₃] showed a decreased intensity of the Raman spectrum, which could be attributed to the introduction of acidic groups into the sample. It is also noteworthy that the position and shape of each peak in the Raman spectrum does not shift after the introduction of acidic groups into GNC. This indicates that the graphene-like nanosheet structure was well maintained in GNC-[C₃N][SO₃CF₃], in good agreement with XRD results.

Table 1 presents the parameters of various acid catalysts. GNC-[C₃N][SO₃CF₃] showed the content of acidic sites at 1.25 mmol g⁻¹, lower than those of various acid catalysts including SBA-15-SO₃H (1.98 mmol g⁻¹), H₃PW₁₂O₄₀ (3.5 mmol g⁻¹), Amberlyst 15 (4.3 mmol g⁻¹) and H₂SO₄ (10.2 mmol g⁻¹). Alternatively, the BET surface area of GNC-[C₃N][SO₃CF₃] (184 m² g⁻¹, Fig. S1†) was higher than that of acidic resin of Amberlyst 15 (45 m² g⁻¹). Compared to the GNC support (945 m² g⁻¹), the decreased surface area in GNC-[C₃N][SO₃CF₃] should result from the grafting of acid active sites, which largely increases the weight of the GNC network. Previously, similar results have also been reported.³⁹

In order to obtain the relationship between the catalyst structure and reactive activity, the surface morphology of the GNC-[C₃N][SO₃CF₃] was analyzed in detail by the multiple image techniques (TEM, HR-TEM and AFM images).

Table 1 The textural and acidic parameters of various catalysts

Samples	Acid contents ^a (mmol g ⁻¹)	N content ^a (mmol g ⁻¹)	S _{BET} ^b (m ² g ⁻¹)	V _p ^b (cm ³ g ⁻¹)	D _p ^c (nm)
GNC	—	1.82	945	3.1	3.8 & 33.7
GNC-[C ₃ N][SO ₃ CF ₃]	1.25	1.57	184	0.59	3.6 & 31.2
GNC-[C ₃ N][SO ₃ CF ₃] ^d	1.22	1.62	173	0.55	3.4 & 30.2
SBA-15-SO ₃ H	1.98	—	814	1.4	7.5
H ₃ PW ₁₂ O ₄₀ ^e	3.50	—	4.2	—	—
Amberlyst 15	4.30	—	45	0.31	40
[C ₃ vim][SO ₃ CF ₃] ^e	2.96	—	—	—	—
H ₂ SO ₄ ^e	10.20	—	—	—	—

^a The acid contents were measured by CHNS elemental analysis. ^b Pore volumes (V_p) were estimated at relative pressure $p/p_0 \approx 0.98$. ^c Average pore diameters were estimated from the BJH model. ^d GNC-[C₃N][SO₃CF₃] after being recycled five times in transesterification of sunflower oil with methanol. ^e The acid contents of H₃PW₁₂O₄₀, [C₃vim][SO₃CF₃] and H₂SO₄ were calculated from the molecular formula.

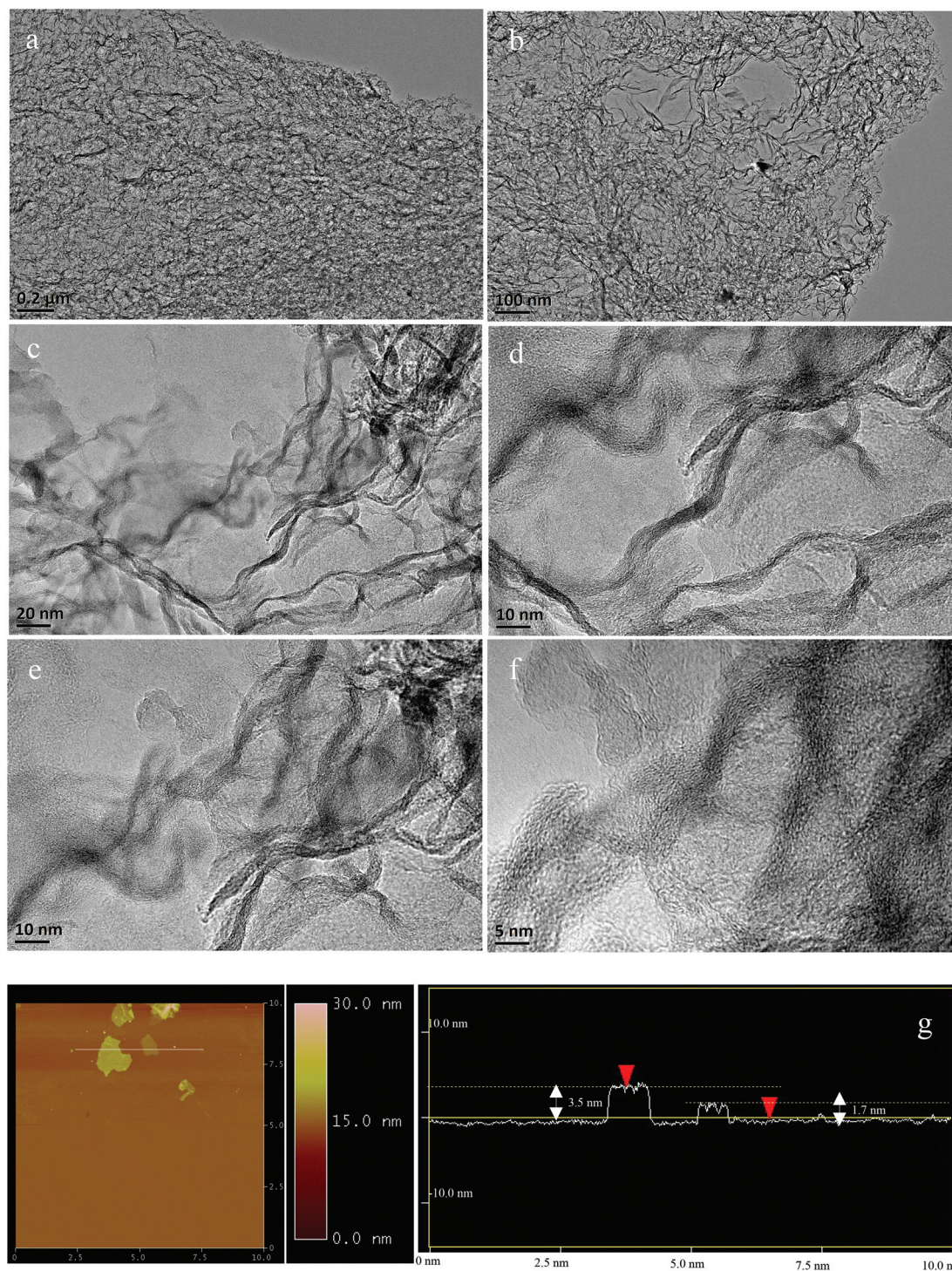


Fig. 2 (a, b) TEM images, (c–f) high-resolved TEM images, and (g) AFM image and corresponding thickness analysis of GNC-[C₃N][SO₃CF₃].

Typically, TEM images indicate a typical nanosheet structure with three dimensional network clusters in GNC-[C₃N]-[SO₃CF₃], exhibiting abundant nanoporous and hollow structures (Fig. 2a, b and S2[†]). Furthermore, highly-resolved TEM images were also used to confirm the graphene structure with crumpled and entangled character (Fig. 2c–f and S1[†]), exhibiting several nanocrystallites with well-defined lattice

planes. When the XRD and Raman aforementioned were combined with TEM and HR-TEM, the uniform graphitized networks were determined. In the meantime, the AFM image of GNC-[C₃N][SO₃CF₃] further affirms its nanosheet structure (Fig. 2g). The thickness of layers ranged from 1.7 to 3.5 nm, indicating the stack had several graphene layers in GNC-[C₃N]-[SO₃CF₃]. These results confirmed that the graphene-like

nanoporous carbon network was formed in GNC-[C₃N]-[SO₃CF₃].

Fig. 3 shows the X-ray photoelectron spectroscopy (XPS) spectra of GNC-[C₃N][SO₃CF₃], which exhibits the signals of S_{2p} (168.8 eV), C_{1s} (284.8 eV), N_{1s} (402.1 eV), O_{1s} (532.4 eV) and F_{1s} (686.8 eV). Notably, the broad C_{1s} spectrum could be fitted and deconvoluted into four peaks, centered at approximately 284.8, 286.1, 287.0 and 292.3 eV, which should be assigned to

C-C and C-N in the GNC network, and C-O and C-F in the strongly acidic ionic liquids and sulfonic group.⁸ In the meantime, the N_{1s} spectrum could be fitted and deconvoluted into two peaks, centered at approximately 398.4, 400.4 and 401.8 eV, which should be assigned to the C-N, N⁺-C₃ ionic liquid group and the protonated structure of GNC-[N⁺H][SO₃CF₃] in GNC-[C₃N][SO₃CF₃].⁸ Similarly, the O_{1s} associated with O-S (531.9 eV) and O-SCF₃ (533.1 eV) could also be observed.⁸

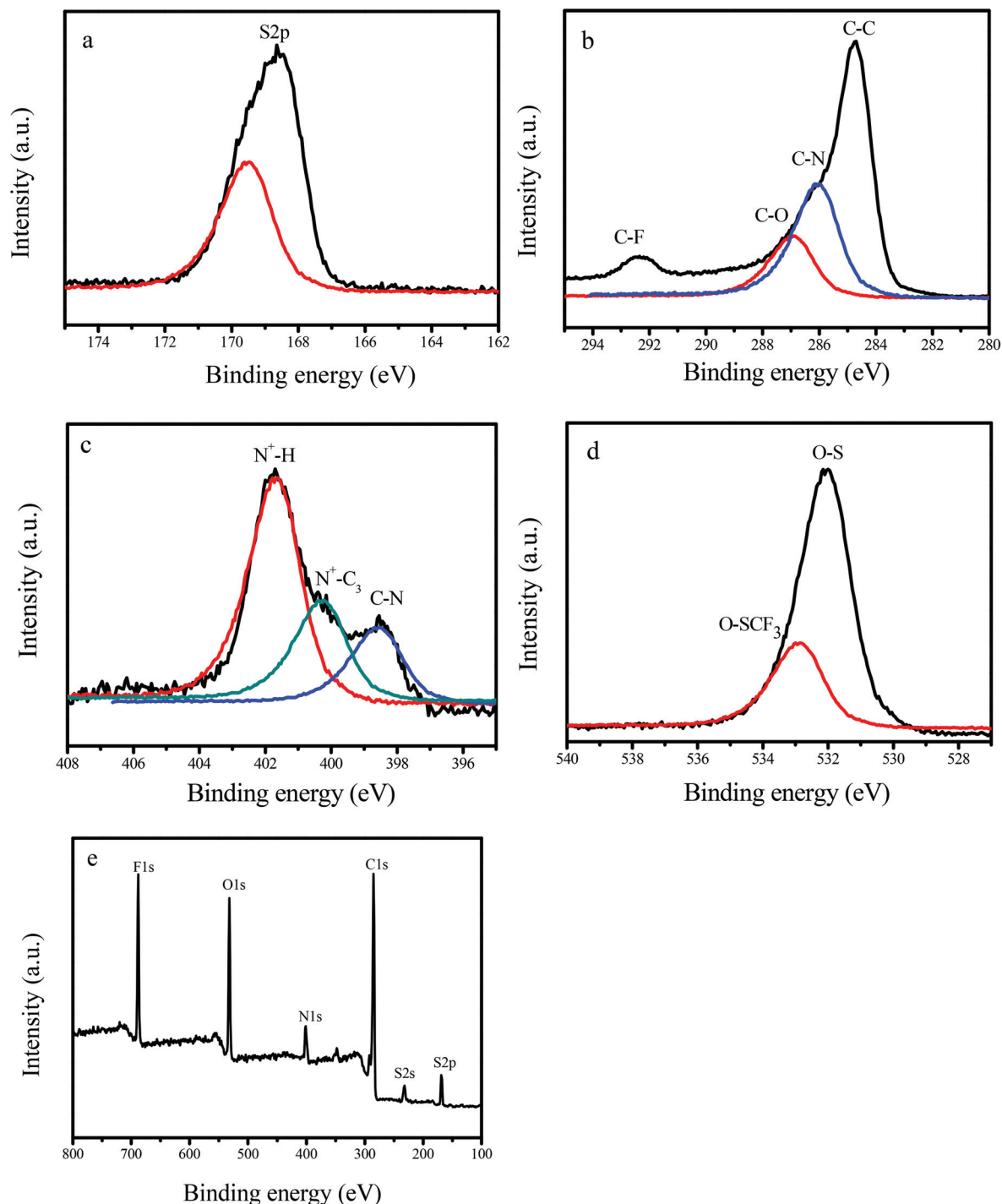


Fig. 3 XPS spectra of (a) S_{2p}, (b) C_{1s}, (c) N_{1s}, (d) O_{1s} and (e) survey of GNC-[C₃N][SO₃CF₃].

The above results confirm that strongly acidic ionic liquids and sulfonic groups have been successfully grafted onto the network of GNCs, in good agreement with FT-IR and elemental analysis results (Fig. S3† & Table 1).

Furthermore, the acidity properties of GNC-[C₃N][SO₃CF₃] were also characterized by the ³¹P NMR probe techniques involving the adsorbed trimethylphosphine (TMP) and trimethylphosphine oxygen (TMPO). It is noteworthy that the ³¹P NMR probe technique is a sensitive and reliable technique to determine the acid type (Brønsted or Lewis acid) and acid strength of solid acid catalysts.^{42–44} As shown in Fig. 4a, using TMP as a probe molecule, the ³¹P resonances at –3.2 ppm were assigned to the protonated adducts of [(CH₃)₃P-H]⁺, and attributed to the reaction of TMP with the Brønsted acidic protons. In contrast, almost no resonances were observed in the range of –20 to –60 ppm due to the interaction with Lewis acid sites.^{42,43} Therefore, it is indicative that no Lewis acid was formed over GNC-[C₃N][SO₃CF₃]. As aforementioned in the Introduction, solid-state ³¹P MAS NMR of adsorbed TMPO is an efficient technique for acidity characterization of solid acid catalysts such as zeolites, sulfated mesoporous metal oxides and heteropolyacids.^{42,43} Interestingly, GNC-[C₃N][SO₃CF₃] showed multiple ³¹P resonance peaks at approximately 45, 48, 51.2, 52.8, 54.5, 56.6 and 63.1 ppm, indicating the presence of various Brønsted acid sites with different acid strengths in GNC-[C₃N][SO₃CF₃] (Fig. 4b). The weakly acidic sites (45 & 48 ppm) may be attributed to the presence of the carboxylic or hydroxyl group in GNC-[C₃N][SO₃CF₃]. While the relatively strongly acidic sites (51.2, 52.8, 54.5, 56.6 and 63.1 ppm) should be attributed to the strong acid ionic liquids, sulfonic group and protonated structure of GNC-[N⁺H][SO₃CF₃] located in the outer and inner surfaces of GNC-[C₃N][SO₃CF₃]. The GNC-[N⁺H][SO₃CF₃] structure should be formed from protonation of the N atom in GNC by HSO₃CF₃. It is noteworthy that the acidity of the –SO₃H group is stronger than GNC-[N⁺H][SO₃CF₃], and the –SO₃H group has a better catalytic role for its activity. The strongly acidic sites in GNC-[C₃N][SO₃CF₃] showed a similar acid strength to that of HY zeolites (55 and 65 ppm) and bifunctional carbon–silica nano composited solid acid (40–70 ppm).^{44,45}

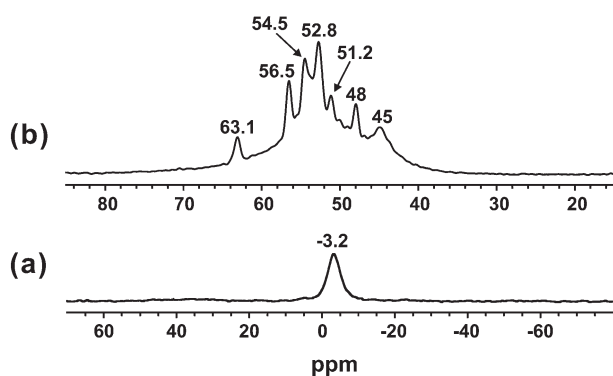


Fig. 4 Room temperature ³¹P MAS NMR spectra of adsorbed (a) TMP acquired with proton decoupling, and (b) TMPO of GNC-[C₃N][SO₃CF₃].

3.2 Catalytic reactions

3.2.1 Towards transesterification to biodiesel. Fig. 5 shows the dependences of catalytic activities on the time in transesterification of tripalmitin with methanol catalyzed by various samples. Notably, GNC-[C₃N][SO₃CF₃] showed much better catalytic activity than those of H₃PW₁₂O₄₀, SBA-15-SO₃H and Amberlyst 15. For instance, the yield of biodiesel (methyl palmitate) catalyzed by GNC-[C₃N][SO₃CF₃] was up to 78.8% after 10 h of reaction, much higher than those of H₃PW₁₂O₄₀ (51.6%), SBA-15-SO₃H (50.5%) and Amberlyst 15 (39.7%). Increasing the reaction time up to 14 h, the yield of methyl palmitate catalyzed by GNC-[C₃N][SO₃CF₃] was increased up to 88.5%. This was even comparable to that of the homogeneous acid ionic liquid of [C₃vim][SO₃CF₃] (89.8%). In contrast, H₃PW₁₂O₄₀, SBA-15-SO₃H and Amberlyst 15 still gave relatively lower biodiesel yields at 64.1, 60.8 and 53.6%, respectively.

Apart from tripalmitin, GNC-[C₃N][SO₃CF₃] also showed good catalytic activity for the transformation of plant oils such as sunflower oil into biodiesel. Table 2 presents catalytic data on transesterification of sunflower oil with methanol for the production of biodiesel over various catalysts. Interestingly, after 18 h of reaction, the yields of biodiesel including C_{16:0}, C_{18:0}, C_{18:1}, C_{18:2} and C_{27:0} catalyzed by GNC-[C₃N][SO₃CF₃] were almost as high as inside the pure acidic ionic liquid of [C₃vim][SO₃CF₃] (89.1, 94.8, 95.2, 93.1, and 86.7% in homogeneous vs. 88.5, 93.6, 94.7, 92.3 and 81.4% in heterogeneous), which was even comparable to that of H₂SO₄ (87.4, 94.1, 95.9, 94.4 and 82.1%). Therefore, it is clear that the high catalytic reactivity has been well retained. As presented in Table 2, the activity of GNC-[C₃N][SO₃CF₃] was much higher than those of heteropolyacid of H₃PW₁₂O₄₀ (58.9, 59.2, 54.3, 60.1 and 50.9%), Amberlyst 15 (54.8, 50.2, 48.6, 50.5 and 26.4%) and SBA-15-SO₃H (60.9, 56.5, 55.4, 52.6 and 45.7%). The excellent

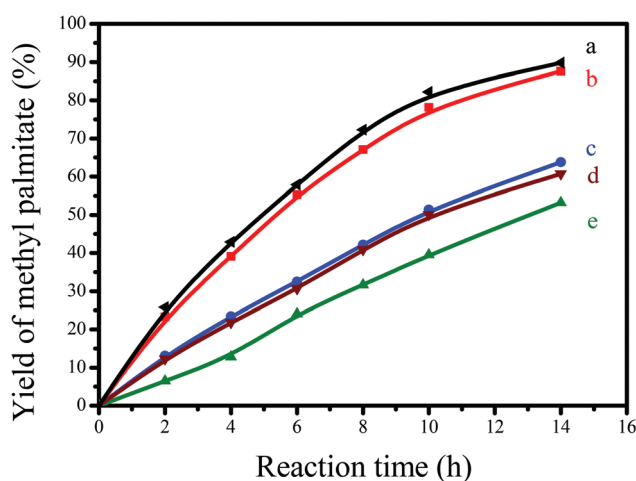


Fig. 5 Dependences of catalytic activities on the time in transesterification of tripalmitin with methanol catalyzed by (a) [C₃vim][SO₃CF₃] (the same number of acidic sites as that of GNC-[C₃N][SO₃CF₃]), (b) GNC-[C₃N][SO₃CF₃], (c) H₃PW₁₂O₄₀, (d) SBA-15-SO₃H and (e) Amberlyst 15. Reaction conditions: 0.84 g tripalmitin; 2.47 mL methanol; 0.1 g catalyst; reaction temperature, 65 °C; reaction time, 14 h.

Table 2 Catalytic data on transesterification of sunflower oil with methanol over various samples^a

Catalysts	Conversion of esters (%)				
	Methyl palmitate (C _{16:0})	Methyl stearate (C _{18:0})	Methyl oleate (C _{18:1})	Methyl linoleate (C _{18:2})	Methyl heptacosane (C _{27:0})
[C ₃ vim][SO ₃ CF ₃] ^b	89.1	94.8	95.2	93.1	86.7
H ₂ SO ₄ ^c	87.4	94.1	95.9	94.4	82.1
GNC-[C ₃ N][SO ₃ CF ₃] ^d	88.5	93.6	94.7	92.3	81.4
GNC-[C ₃ N][SO ₃ CF ₃] ^d	84.3	89.1	92.3	90.7	78.3
H ₃ PW ₁₂ O ₄₀	58.9	59.2	54.3	60.1	50.9
Amberlyst 15	54.8	50.2	48.6	50.5	26.4
SBA-15-SO ₃ H	60.9	56.5	55.4	52.6	45.7

^a 1.0 g sunflower oil; 2.47 mL methanol; 0.15 g catalyst; reaction temperature, 65 °C; reaction time, 18 h. The catalytic activity of the catalysts was characterized quantitatively by the conversion of fatty acid methyl esters (FAME, Y %) which was calculated as follows: Yield = (M_D/M_T) × 100%, where M_D and M_T are the numbers of moles of each FAME produced and expected, respectively. In this section, M_T is the number of moles of FAME catalyzed by 0.2 g of H₂SO₄ for 24 h, which was performed at 65 °C with the same content of feedstock as that of GNC-[C₃N][SO₃CF₃].

^b Imidazole based acidic ionic liquid synthesized using the same procedure as that of GNC-[C₃N][SO₃CF₃]. ^c The same number of acidic sites as that of GNC-[C₃N][SO₃CF₃]. ^d The 5th cycle in transesterification of sunflower oil with methanol.

catalytic activity found in GNC-[C₃N][SO₃CF₃] for biodiesel production could be attributed to its controlled acidity, good dispersion, abundant and hierarchical nanoporosity, and unique nanosheet structure. By themselves, they are capable of enhancing the fast diffusion of reactants and products, increasing the exposure degree of catalytically active sites, in processes of various reactions. Compared to GNC-[C₃N][SO₃CF₃], the low BET surface areas of H₃PW₁₂O₄₀ and Amberlyst 15 resulted in their low exposure degrees and easy poison of active sites, further leading to their low catalytic activities. Although SBA-15-SO₃H has large BET surface areas, its functional group could be easily occluded in the silica wall.⁴⁶ Moreover, the accessibility of reactants to catalytically active sites located into the mesopores of SBA-15-SO₃H is usually difficult in comparison to two dimensional nanosheet structures of GNC-[C₃N][SO₃CF₃].²⁷ These factors resulted in a lower catalytic activity of SBA-15-SO₃H. The above results prove that GNC-[C₃N][SO₃CF₃] could be used as a highly efficient solid acid for biodiesel production.

More importantly, GNC-[C₃N][SO₃CF₃] showed very good recyclability for catalyzing biodiesel production. For example, in the reaction of sunflower oil with methanol, even after being recycled five times, the yields of biodiesel catalyzed by GNC-[C₃N][SO₃CF₃] were still up to 86.2, 90.8, 92.1, 89.4 and 79.5% (Table 2), comparable to fresh GNC-[C₃N][SO₃CF₃] (88.5, 93.6, 94.7, 92.3 and 81.4%, Table 2).

3.2.2 Depolymerization of crystalline cellulose into bio-fuels. To further decrease the cost of biofuels, much effort has been made to develop green and cost-effective ways to produce renewable biofuels from cellulosic biomass, in recent years. The depolymerization of crystalline cellulose (Avicel) into sugars, catalyzed by various acid catalysts, has also been investigated in this work, and was achieved in the presence of 1-*n*-butyl-3-methylimidazolium and DMSO mixed solvents.

Fig. 6 shows the dependences of catalytic activities on the time in depolymerization of Avicel catalyzed by GNC-[C₃N][SO₃CF₃], Amberlyst 15, HCl and [C₃vim][SO₃CF₃]. Notably, GNC-[C₃N][SO₃CF₃] showed significantly better catalytic activity

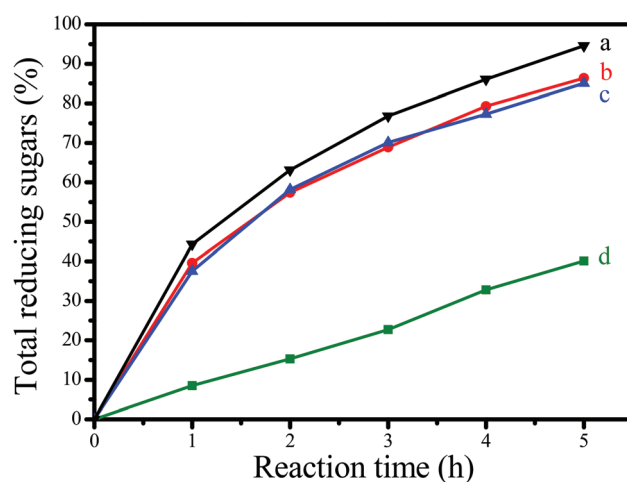


Fig. 6 Dependences of catalytic activities on the time in depolymerization of Avicel into sugars catalyzed by (a) GNC-[C₃N][SO₃CF₃], (b) HCl, (c) [C₃vim][SO₃CF₃] and (d) Amberlyst 15 (b, c, d used the same number of acidic sites as those in GNC-[C₃N][SO₃CF₃]). Reaction conditions: 0.1 g, Avicel; 1.5 g [C₄mim]Cl ionic liquid, and 0.5 mL DMSO mixed solvents; 20 mg catalyst; reaction temperature, 100 °C; reaction time, 5 h. The total reducing sugars were monitored using the 3,5-dinitrosalicylic acid (DNS) reagent.

than that of Amberlyst 15, one of the most efficient commercial acidic resins, comparable to those of homogeneous HCl and [C₃vim][SO₃CF₃] (the same number of active sites as in GNC-[C₃N][SO₃CF₃]). For example, the yields of total reducing sugars, mono- and disaccharides catalyzed by GNC-[C₃N][SO₃CF₃] was 94.6% after 5 h of incubation, higher than those of Amberlyst 15 (40.5%), HCl (87.1%) and [C₃vim][SO₃CF₃] (84.9%). Similar results could also be obtained from HPLC data (as shown in Table 3); the yields of the main products including glucose (44.1%), cellobiose (32.7%) and HMF (11.6%) catalyzed by GNC-[C₃N][SO₃CF₃] were much higher than that of Amberlyst 15 (14.3, 17.5 and 3.2%), which were comparable to those of homogeneous HCl (39.8, 20.4 and 10.7%) and [C₃vim][SO₃CF₃] (26.3, 34.5 and 10.1%). Presumably,

Table 3 Yields of sugars and dehydration products in the depolymerization of Avicel catalyzed by various solid acids^a

Run	Samples	Glucose yield ^b (%)	Cellobiose yield ^b (%)	HMF yield ^b (%)	TRS ^c (%)
1	Amberlyst 15 ^c	14.3	17.5	3.2	40.5
2	HCl ^d	39.8	20.4	10.7	87.1
3	[C ₃ vim][SO ₃ CF ₃] ^d	26.3	34.5	10.1	84.9
4	GNC-[C ₃ N][SO ₃ CF ₃]	44.1	32.7	11.6	94.6

^a 0.1 g Avicel; 1.5 g [C₄mim]Cl ionic liquid, and 0.5 mL DMSO mixed solvents; 20 mg catalyst; reaction temperature, 100 °C; reaction time, 5 h. ^b Measured by the HPLC method. ^c Measured by the DNS method. ^d The same number of acidic sites as in GNC-[C₃N][SO₃CF₃].

the drastic enhancement of the catalytic effectiveness found in GNC-[C₃N][SO₃CF₃] during biomass transformation was attributed to the synergistic effects from the abundant nanopores, unique nanosheet structure, good dispersion, controlled acidity and good network stability of the catalyst.

The preparation of GNC-[C₃N][SO₃CF₃] will open an effective method for synthesizing graphene-like nanoporous carbon based solid acids with excellent catalytic activity and a long life for biomass transformation, which will be potentially important for the wide applications of graphene based nanomaterials in the areas of biofuel exploitation in the near future.

4. Conclusion

Efficient graphene-like nanoporous carbon based solid acids (GNC-SO₃H-ILs) were successfully synthesized and tested for their effectiveness in biomass transformation. GNC-SO₃H-ILs showed controlled acidity, abundant nanopores, unique nanosheet structure and good dispersion in various reaction media, resulting in their excellent catalytic efficiency for biodiesel production and depolymerization of crystalline cellulose into biofuel precursors. The preparation of GNC-SO₃H-ILs will offer a facile and cost-effective way to synthesize nanoporous graphene based solid strong acids, which will be very important for their wide applications in the areas of biofuel production through green and sustainable processes.

Acknowledgements

This work was supported by the National Natural Science Foundation of China (21203122, 21473244 and 21173255), the Foundation of Science, Key Sci-Tech Innovation Team Project of Zhejiang Province (2010R50014-20), Postdoctoral Foundation of China (2012M520062, Bsh1201018), the Foundation of State Key Laboratory of Magnetic Resonance and Atomic and Molecular Physics, Wuhan Institute of Physics and Mathematics, Chinese Academy of Sciences (T151303) and State Key Laboratory of Inorganic Synthesis and Preparative Chemistry, Jilin University (2013-12).

References

- G. W. Huber, S. Iborra and A. Corma, *Chem. Rev.*, 2006, **106**, 4044.
- A. Corma, S. Iborra and A. Velty, *Chem. Rev.*, 2007, **107**, 2411.
- M. Toda, A. Takagaki, M. Okamura, J. N. Kondo, S. Hayashi, K. Domen and M. Hara, *Nature*, 2005, **438**, 178.
- Y. Román-Leshkov, C. J. Barrett, Z. Y. Liu and J. Dumesic, *Nature*, 2007, **447**, 982.
- G. W. Huber, J. N. Chheda, C. J. Barrett and J. A. Dumesic, *Science*, 2005, **308**, 1446.
- Y. Román-Leshkov, J. N. Chheda and J. A. Dumesic, *Science*, 2006, **312**, 1933.
- R. Rinaldi and F. Schüth, *ChemSusChem*, 2009, **2**, 1096.
- F. J. Liu, L. Wang, Q. Sun, L. F. Zhu, X. J. Meng and F.-S. Xiao, *J. Am. Chem. Soc.*, 2012, **134**, 16948.
- F. J. Liu, R. K. Kamat, I. Noshadi, D. Peck, R. S. Parnas, A. Zheng, C. Qi and Y. Lin, *Chem. Commun.*, 2013, **49**, 8456.
- J. B. Binder and R. T. Raines, *J. Am. Chem. Soc.*, 2009, **131**, 1979.
- F. J. Liu, A. M. Zheng, I. Noshadi and F.-S. Xiao, *Appl. Catal., B*, 2013, **136–137**, 193.
- J. B. Binder and R. T. Raines, *Proc. Natl. Acad. Sci. U. S. A.*, 2010, **107**, 4516.
- L. Wang, H. Wang, F. J. Liu, A. Zheng, J. Zhang, Q. Sun, J. P. Lewis, L. Zhu, X. Meng and F.-S. Xiao, *ChemSusChem*, 2014, **7**, 402.
- R. Rinaldi, R. Palkovits and F. Schüth, *Angew. Chem., Int. Ed.*, 2008, **47**, 8047.
- F. M. A. Geilen, B. Engendahl, A. Harwardt, W. Marquardt, J. Klankermayer and W. Leitner, *Angew. Chem., Int. Ed.*, 2010, **49**, 5510.
- I. Noshadi, B. Kanjilal, S. C. Du, G. M. Bollas, S. L. Suib, A. Provasat, F. J. Liu and R. S. Parnas, *Appl. Energy*, 2014, **129**, 112.
- A. Corma, *Chem. Rev.*, 1997, **97**, 2373.
- F. Su and Y. H. Guo, *Green Chem.*, 2014, **16**, 2934.
- H. L. Cai, C. Z. Li, A. Q. Wang, G. L. Xu and T. Zhang, *Appl. Catal., B*, 2012, **123–124**, 333.
- S. Sukanuma, K. Nakajima, M. Kitano, D. Yamaguchi, H. Kato, S. Hayashi and M. Hara, *J. Am. Chem. Soc.*, 2008, **130**, 12787.
- M. Hara, T. Yoshida, A. Takagaki, T. Takata, J. N. Kondo, S. Hayashi and K. Domen, *Angew. Chem., Int. Ed.*, 2004, **43**, 2955.
- R. Xing, Y. M. Liu, Y. Wang, L. Chen, H. H. Wu, Y. W. Jiang, M. Y. He and P. Wu, *Microporous Mesoporous Mater.*, 2007, **105**, 41.
- Z. X. Ding, X. F. Chen, M. Antonietti and X. C. Wang, *ChemSusChem*, 2011, **4**, 274.
- Y. Zhang, A. Thomas, M. Antonietti and X. Wang, *J. Am. Chem. Soc.*, 2009, **131**, 50.
- K. S. Novoselov, A. K. Geim, S. V. Morozov, D. Jiang, Y. Zhang, S. V. Dubonos, I. V. Grigorieva and A. A. Firsov, *Science*, 2004, **306**, 666.

- 26 A. K. Geim, *Science*, 2009, **324**, 1530.
- 27 K. S. Novoselov, A. K. Geim, S. V. Morozov, D. Jiang, M. I. Katsnelson, I. V. Grigorieva, S. V. Dubonos and A. A. Firsov, *Nature*, 2005, **438**, 197.
- 28 M. A. Worsley, P. J. Pauzuskie, T. Y. Olson, J. Biener, J. H. Satcher Jr. and T. F. Baumann, *J. Am. Chem. Soc.*, 2010, **132**, 14067.
- 29 S. B. Yang, X. L. Feng, X. C. Wang and K. Müllen, *Angew. Chem., Int. Ed.*, 2011, **50**, 5339.
- 30 X.-H. Li, J.-S. Chen, X. C. Wang, M. E. Schuster, R. Schlögl and M. Antonietti, *ChemSusChem*, 2012, **5**, 642.
- 31 F. J. Liu, J. Sun, L. F. Zhu, X. J. Meng, C. Z. Qi and F.-S. Xiao, *J. Mater. Chem.*, 2012, **22**, 5495.
- 32 P. P. Upare, J.-W. Yoon, M. Y. Kim, H.-Y. Kang, D. W. Hwang, Y. K. Hwang, H. H. Kung and J.-S. Chang, *Green Chem.*, 2013, **15**, 2935.
- 33 H. L. Wang, T. S. Deng, Y. X. Wang, X. J. Cui, Y. Q. Qi, X. D. Mu, X. L. Hou and Y. L. Zhu, *Green Chem.*, 2013, **15**, 2379.
- 34 J.-S. Lee, S.-I. Kim, J.-C. Yoon and J.-H. Jang, *ACS Nano*, 2013, **7**, 6047.
- 35 Y. Zhu, S. Murali, M. D. Stoller, K. J. Ganesh, W. Cai, P. J. Ferreira, A. Pirkle, R. M. Wallace, K. A. Cychosz, M. Thommes, D. S. Su, E. A. Stach and R. S. Ruoff, *Science*, 2011, **332**, 1537.
- 36 Z. Chen, W. Ren, L. Gao, B. Liu, S. Pei and H.-M. Cheng, *Nat. Mater.*, 2011, **10**, 424.
- 37 X.-H. Li, S. Kurasch, U. Kaiser and M. Antonietti, *Angew. Chem., Int. Ed.*, 2012, **51**, 9689.
- 38 Z. G. Xiong, L. L. Zhang and X. S. Zhao, *Chem. – Eur. J.*, 2011, **17**, 2428.
- 39 D. Margolese, J. A. Melero, S. C. Christiansen, B. F. Chmelka and G. D. Stucky, *Chem. Mater.*, 2000, **12**, 2448.
- 40 A. C. Ferrari and D. M. Basko, *Nat. Nanotechnol.*, 2013, **8**, 235.
- 41 A. C. Ferrari, J. C. Meyer, V. Scardaci, C. Casiraghi, M. Lazzeri, F. Mauri, S. Piscanec, D. Jiang, K. S. Novoselov, S. Roth and A. K. Geim, *Phys. Rev. Lett.*, 2006, **97**, 187401.
- 42 A. Zheng, S. J. Huang, S. B. Liu and F. Deng, *Phys. Chem. Chem. Phys.*, 2011, **13**, 14889.
- 43 Y. Chu, Z. Yu, A. Zheng, H. Fang, H. Zhang, S. J. Huang, S. B. Liu and F. Deng, *J. Phys. Chem. C*, 2011, **115**, 7660.
- 44 M. D. Karra, K. J. Sutovich and K. T. Mueller, *J. Am. Chem. Soc.*, 2002, **124**, 902.
- 45 F. de Clippel, M. Dusselier, R. V. Rompaey, P. Vanelderden, J. Dijkmans, E. Makshina, L. Giebel, S. Oswald, G. V. Baron, J. F. M. Denayer, P. P. Pescarmona, P. A. Jacobs and B. F. Sels, *J. Am. Chem. Soc.*, 2012, **134**, 10089.
- 46 T. Yokoi, H. Yoshitake, T. Yamada, Y. Kubota and T. Tatsumi, *J. Mater. Chem.*, 2006, **16**, 1125.